SUPPLEMENTARY INFORMATION
Disentangling the Functional Consequences of the Connectivity between Optic-Flow Processing Neurons

F. Weber[1,2], C.K. Machens[3,4], and A. Borst[1]

[1]Department of Systems and Computational Neurobiology, Max-Planck-Institute of Neurobiology, Martinsried, Germany
[2]Graduate School of Systemic Neurosciences, Ludwig-Maximilians-University Munich, Germany
[3]Group for Neural Theory, INSERM Unité 960, École Normale Supérieure, Département d'Etudes Cognitives, Paris, France
[4]*Present Address*: Champalimaud Neuroscience Program, Champalimaud Foundation, Lisbon, Portugal

E-mail: `weberf@neuro.mpg.de`

Nature Neuroscience doi:10.1038/nn.3044

This document contains Supplementary Information related to the manuscript 'Disentangling the Functional Consequences of the Connectivity between Optic-Flow Processing Neurons'. The Supplementary Information is organized into two Sections: In Section A (Supplementary Figures), we present Supplementary Figures complementing the data presented in the main text. In Section B (Supplementary Results), we discuss a linear two-neuron model, which reproduces phenomena of the recorded data and predictions by the generalized linear models.

A. Supplementary Figures

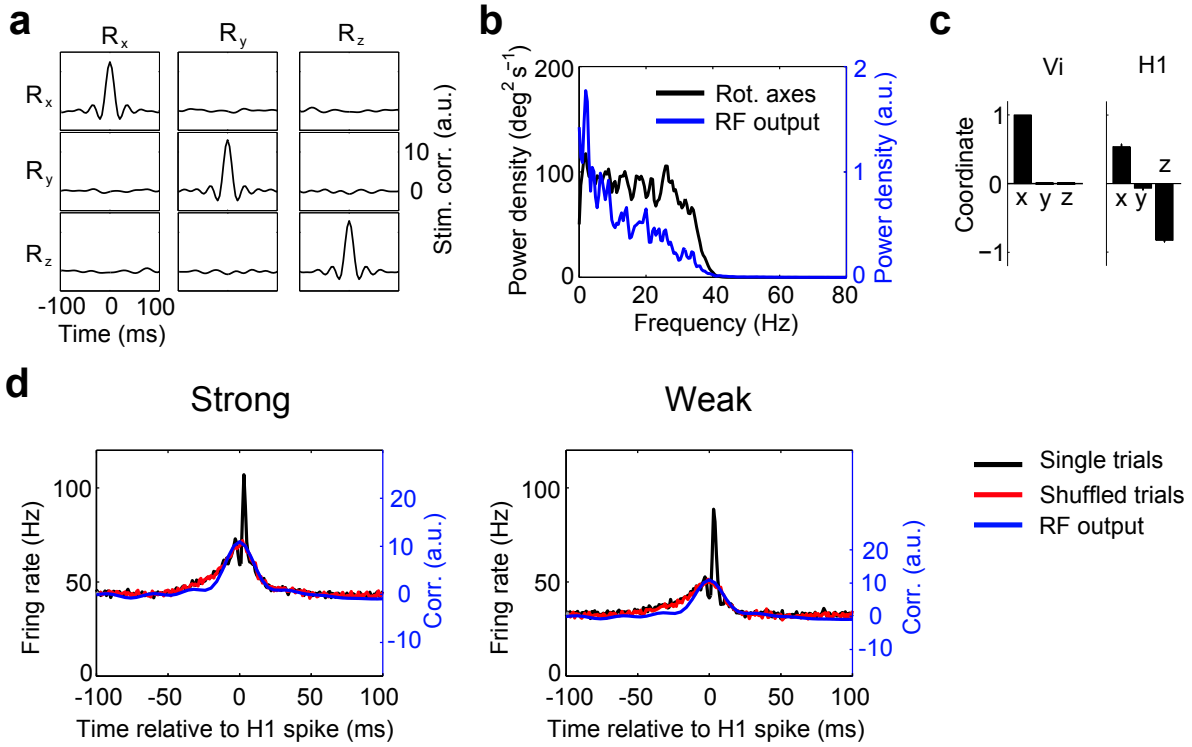

Supplementary Figure 1 (related to Figure 2)
Stimulus Statistics.
(a) Auto- and cross-correlations of the x-, y-, and z-rotation velocity (denoted by R_x, R_y, and R_z).
(b) The averaged power spectra of R_x, R_y, and R_z are shown in black. The power spectrum of the one-dimensional input signal for the GLM (RF Output) is shown in blue. This signal is obtained from projecting the Reichardt detector array response (elicited by the strong stimulus) onto Vi's receptive field. The Reichardt detector array acts as low-pass filter.
(c) Coordinates of Vi and H1 in the rotated (orthogonal) coordinate system, where the x-axis is aligned with Vi's preferred rotation axis. H1's preferred rotation axis is a linear combination of the x- and z-axis. Since H1 is sensitive to x-rotations, both neurons are stimulus correlated. Moreover, the preferred rotation axes of both Vi and H1 are orthogonal to the y-axis.
(d) Correlation analysis for Vi and H1. The cross-correlations of simultaneously recorded spike trains of Vi and H1 are shown in black for both strong (left) and weak stimulation (right). The response correlation obtained for shuffled trials is shown in red. This cross-correlation reflects correlations induced by the stimulus. Hence, the slow positive correlation in the single trial cross-correlation (black) is induced by the stimulus, while the short peak reflects a fast synaptic interaction between Vi and H1. The cross-correlation of the one-dimensional input signals for Vi's and H1's GLM exhibits a similar

shape as the shuffled cross-correlation (blue, RF Output), which is a further indication that the slow component in the single trial cross-correlation is due to correlated inputs to Vi and H1.

Nature Neuroscience doi:10.1038/nn.3044

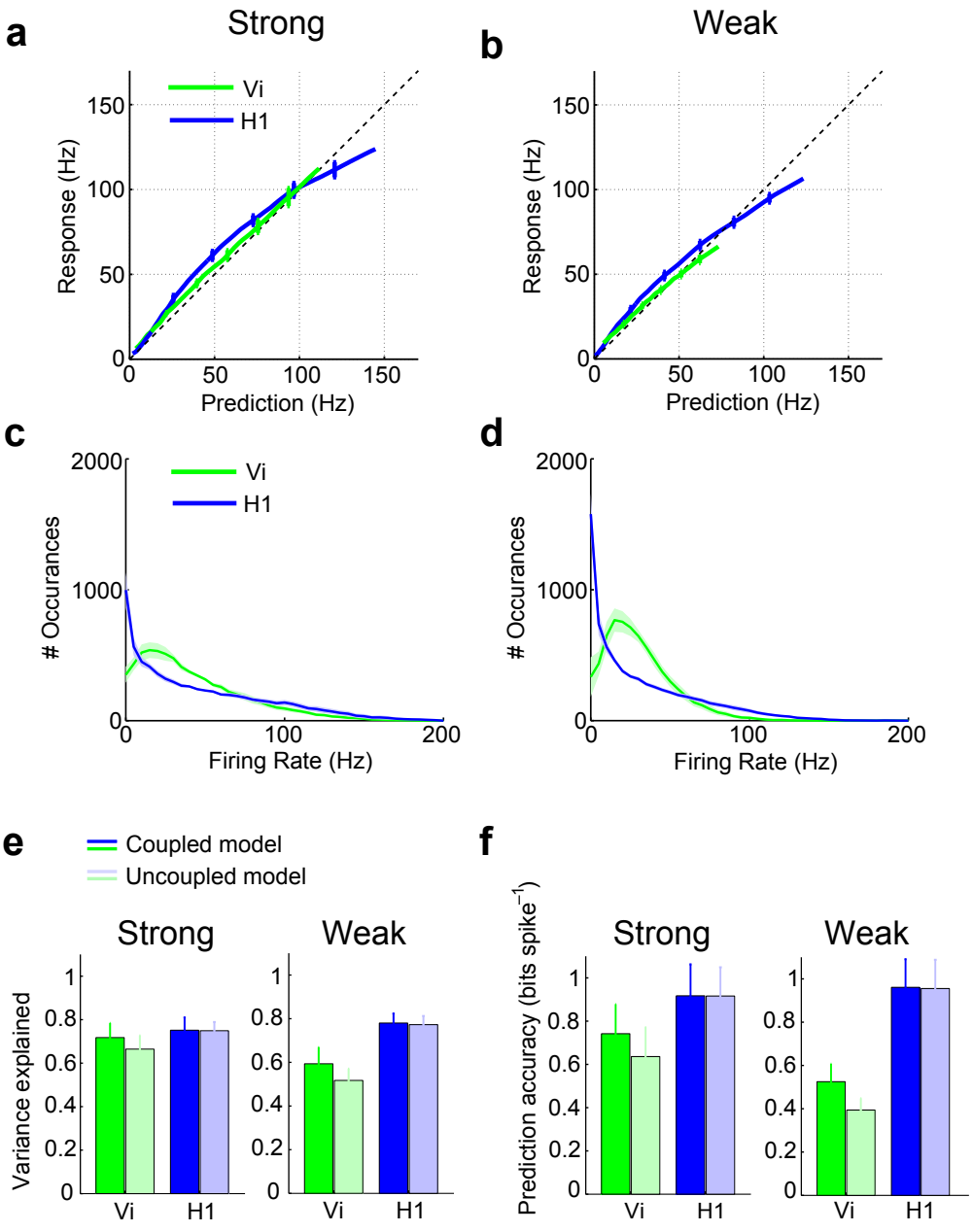

Supplementary Figure 2 (related to Figure 3)
Evaluation of the GLM for Vi and H1.
(a,b) Calibration plots for weak **(a)** and strong stimulation **(b)**. In each calibration plot, the firing rate predicted by the GLM is plotted against the measured firing rate. Especially for Vi (green), the resulting curve falls onto the identity line demonstrating that, for this cell, the exponential function is a good description for the spiking nonlinearity. For H1 (blue), the calibration curve has a slightly concave shape. Thus for small firing rates, H1's spiking nonlinearity is steeper than the exponential, whereas for large firing rates ($>$ 100 Hz) the spiking nonlinearity becomes shallower than the exponential. Error bars denote the S.E.M (n=8).
(c,d) Averaged histograms showing the distribution of firing rates of Vi and H1 for

weak **(c)** and strong stimulation **(d)**. The green and blue shadings depict the S.E.M. for Vi and H1.

(e,f) Evaluation of the coupled and uncoupled GLM for Vi and H1 during weak and strong stimulation. The performance of the coupled GLM (as introduced in Fig. 3a) was compared to the performance of an uncoupled GLM, where the firing rate only depends on the stimulus and the post-spike filter. Models were trained on the uncorrelated random rotation stimulus and evaluated on the correlated stimulus (see Methods). To quantify the models, we determined the variance in the recorded firing rates explained by the GLM **(e)** or the prediction accuracy of the respective model **(f)**. The prediction accuracy is defined in Methods. For the GLM, the firing rates were calculated by averaging the spike trains predicted for repeated presentation of the stimulus.

(e) Variance explained by the coupled and uncoupled models. For Vi, the variance explained by the uncoupled model is reduced, whereas for H1 the performance is unchanged for both models.

(f) Prediction accuracy of the coupled and uncoupled models (measured in bits spike^{-1}). As for the variance explained, the prediction accuracy of the uncoupled model for Vi is reduced, while H1's performance does not depend on Vi.

Nature Neuroscience doi:10.1038/nn.3044

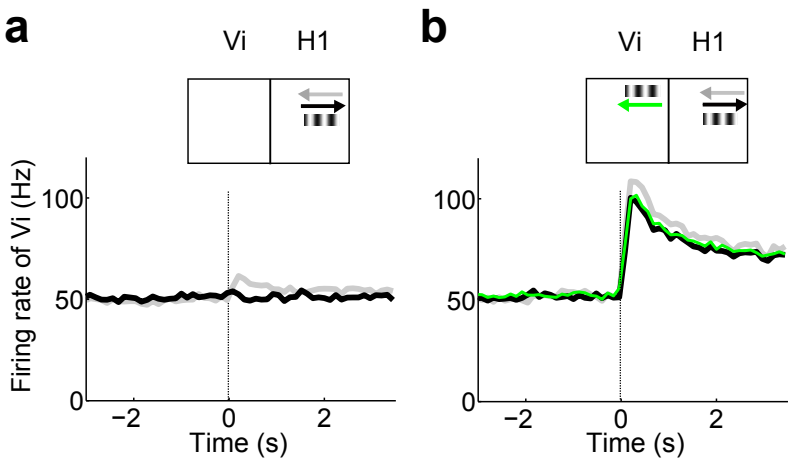

Supplementary Figure 3 (related to Figure 5)
Control Experiments for Unilateral Stimulation.
(a) To inhibit H1 during unilateral stimulation of Vi (see Fig. 5e), we presented a small sine grating on the right half of the stimulation screen. To exclude that this grating inhibits Vi, we recorded Vi's activity, while only presenting the sine grating at the same position as in Fig. 5e. The upper scheme depicts the location of the sine grating on the stimulus device. The arrows indicate the motion direction of the grating. To maximally increase Vi's spontaneous activity, the area outside the sine grating was constantly fully illuminated. If the sine grating moves in H1's preferred direction (indicated by the gray arrow), Vi's activity is slightly increased as expected from the uni-directional, excitatory coupling revealed by the GLM (gray line). Contrarily, if the grating moves in H1's null direction (black arrow), Vi's firing rate is unaffected (black line). Hence, the grating does not inhibit Vi. The grating started moving at 0 s at a constant temporal frequency of 1.5 Hz ($n = 7$ flies).
(b) In a further control experiment, we excluded shunting inhibition of Vi. Here, Vi was excited on the left side of visual space by a small grating moving left-to-right (see upper scheme), while a small sine grating was moving on the right side in H1's preferred or null direction. Three cases were compared: (1) Only the left grating moves left-to-right (green). (2) The left grating moves left-to-right, while the right pattern moves in H1's preferred direction (gray). (3) The left grating moves left-to-right, while the right pattern moves in H1's null direction (black). Note that in all three cases the left grating moved from left-to-right, thereby exciting Vi. If the right grating moved in H1's preferred direction, Vi's firing rate was slightly increased (gray). Since the firing rates for the remaining two cases overlap (black and green), it can be excluded that the right grating had an inhibitory effect on Vi (n=7 flies).

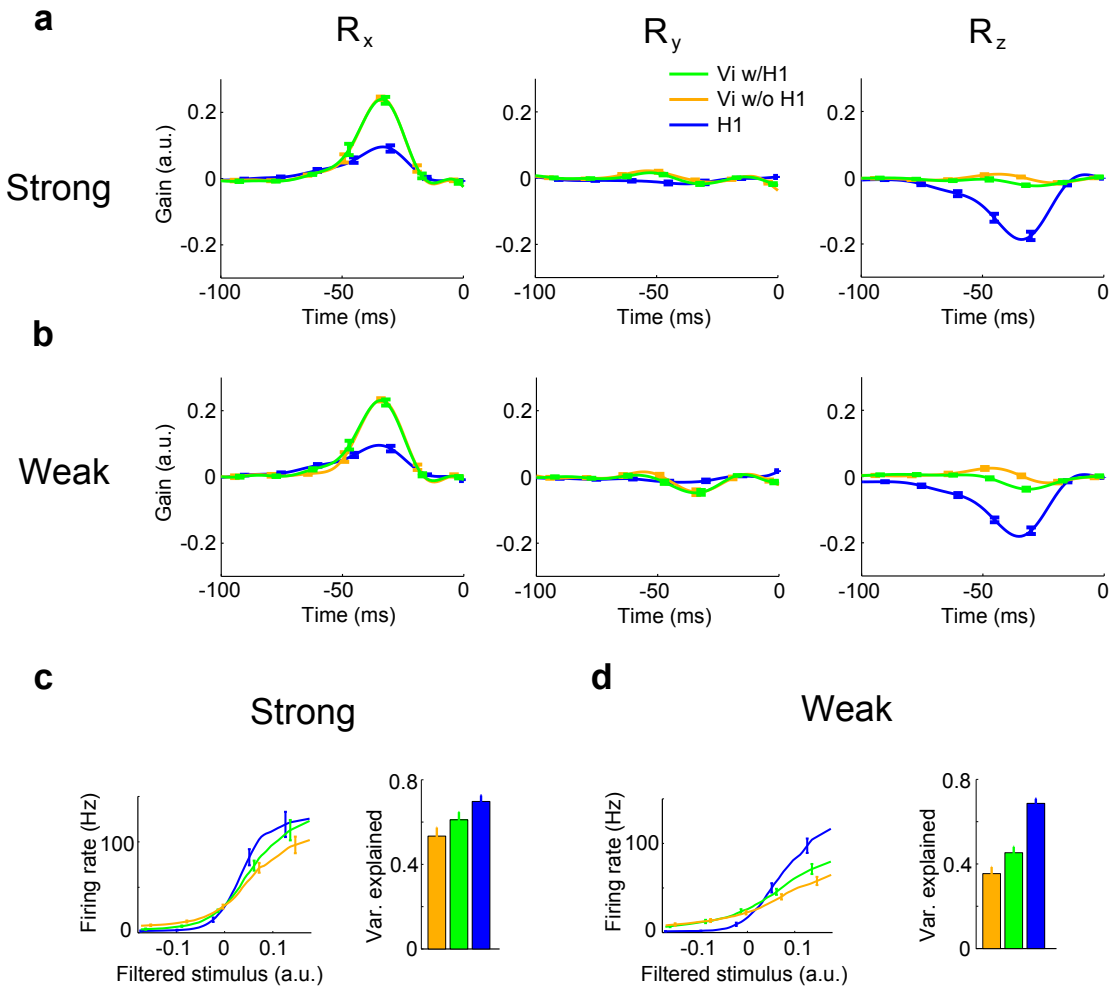

Supplementary Figure 4 (related to Figure 5)
Linear-Nonlinear Model for Bilateral and Unilateral Stimulation.
(a,b) Linear Components of linear-nonlinear (LN) models mapping the three-dimensional rotation profile onto the recorded firing rates. Since the stimulus is three-dimensional, the linear filter stage comprises three components filtering the x-, y-, and z-rotation velocity (denoted by R_x, R_y, and R_z). Since we rotated the coordinate system such that Vi's preferred rotation axis is aligned with the x-axis, only Vi's x-rotation filters are significantly different from zero. The filters of the LN-model for Vi mapping the rotation profile onto the response recorded during bilateral stimulation are shown in green. We compared these components to the filters of the LN-model transforming the stimulus to the response recorded during unilateral stimulation of Vi (orange), while H1 was silenced by a small moving grating (see Fig. 5e). The filters for both models strongly overlap indicating that Vi's stimulus tuning is nearly unaffected by inputs from the contralateral lobula plate. The small difference in the z-filters of the LN-models for uni- and bilateral stimulation indicates the presence of a contralateral interaction partner of Vi which is sensitive to negative z-rotations, as it is the case for H1. For comparison, the LN-model for H1 is shown in blue. The small change in the

z-filters is complementary to the tiny, though significant shift of Vi's stimulus tuning in Fig 5a,b, similarly indicating contralateral inputs to Vi by a neuron tuned to z-rotations. **(c,d)** While bilateral stimulation (and therefore inputs from the contralateral H1) leave the stimulus filters nearly unaffected, the nonlinearity of Vi is modulated by contralateral input: During strong and weak stimulation, the slope (gain) of the nonlinearity is increased (left). Moreover, the firing rates elicited by bilateral stimulation can be better predicted compared to unilateral stimulation as quantified by the variance explained in the recorded data (right).

Nature Neuroscience doi:10.1038/nn.3044

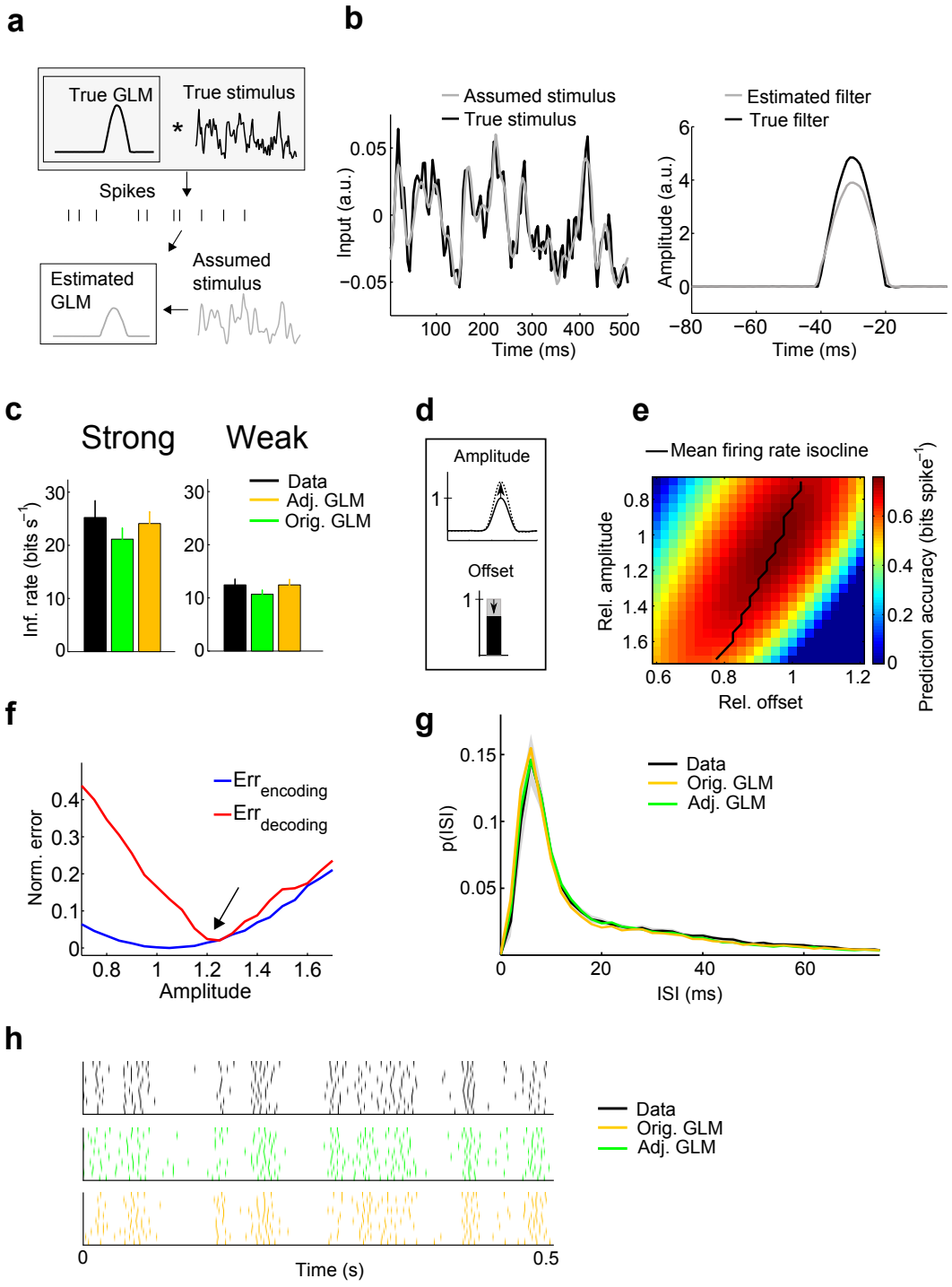

Supplementary Figure 5 (related to Figure 6)
Adjusting the GLM's Stimulus Amplitude.

(**a**) If the true stimulus, provided by pre-synaptic elements to the recorded cell, is unknown, the GLM under-estimates the amplitude of the stimulus filter. To demonstrate this effect, we generated spikes by a GLM referred to as the 'true' GLM. The stimulus filter of this 'true' GLM and the 'true' stimulus are shown in the gray box. We then tested, if the 'true' stimulus filter can be recovered. In case the 'true' stimulus is

known (and if enough data is available) this is perfectly possible. However, for a real neuron, the 'true' stimulus, i.e. the exact input provided by pre-synaptic elements to the neuron, is unknown. Instead, we have to assume a stimulus which approximates the 'true' stimulus. The 'assumed' stimulus used for the estimation of the GLM is depicted in gray. It was generated by low-pass filtering the 'true' stimulus. The amplitude of the stimulus filter of the 'estimated' GLM is under-estimated (gray).
(b) (Left) Overlay of the 'true' and 'assumed' stimulus. (Right) The 'true' and 'estimated' filter. The 'estimated' filter has a smaller amplitude than the 'true' one.
(c) The optimal encoding model (Orig. GLM, green) under-estimates the information carried by the recorded spikes of Vi (Data, black) about x-rotations. Adjusting the GLM's amplitude allows compensating for this bias (Adj. GLM, orange). The information was estimated using linear decoding (see Methods). Error bars denote the S.E.M.
(d) Scheme illustrating the adjustment of the GLM. To compensate for the under-estimated decoding performance of the GLM, we increased the amplitude of the stimulus filter. To match the mean firing rate we reduced the offset parameter.
(e) Averaged prediction accuracy of Vi (measured in bits spike^{-1}) for strong stimulation as function of the stimulus filter amplitude and the offset parameter. For both parameters, the x- or y-axis depicts the factor by which the amplitude or offset of the original GLM was changed (relative amplitude or relative offset). Hence, 1 corresponds to the parameter values of the original GLM. All models which preserve the measured mean firing rate lie on the black line (Mean Firing Rate Isocline).
(f) Encoding and decoding error in dependence of the stimulus filter amplitude (for strong stimulation). The blue curve shows the averaged percentage deviation from the prediction accuracy maximum (measured in bits spike^{-1}) along the mean firing rate isocline in **(e)**. The red curve quantifies the percentage by which the information (measured in bits spike^{-1}) of the simulated spikes deviates from the information carried by the recorded spikes. As new stimulus filter amplitude, we chose the value that minimizes the sum of both errors (indicated by the arrow). The x-axis depicts the factor by which the stimulus filter amplitude was changed.
(g) Comparison of the inter-spike interval (ISI) distribution of the recorded spikes (black) with the distributions of the spikes predicted by the original (green) and adjusted GLM (orange). Although adjusting the amplitude slightly increased the peak of the interval distribution at 8ms, all three curves still closely overlap. Hence, the correction only slightly affects the predicted responses. The gray shading depicts the S.E.M. of the recorded data. **(h)** Spike responses of a single Vi cell to repeated presentation of a 0.5 s stimulus segment of strong stimulation. The recorded spike trains are shown in black. The responses generated by the original and adjusted GLM are shown in green and orange.

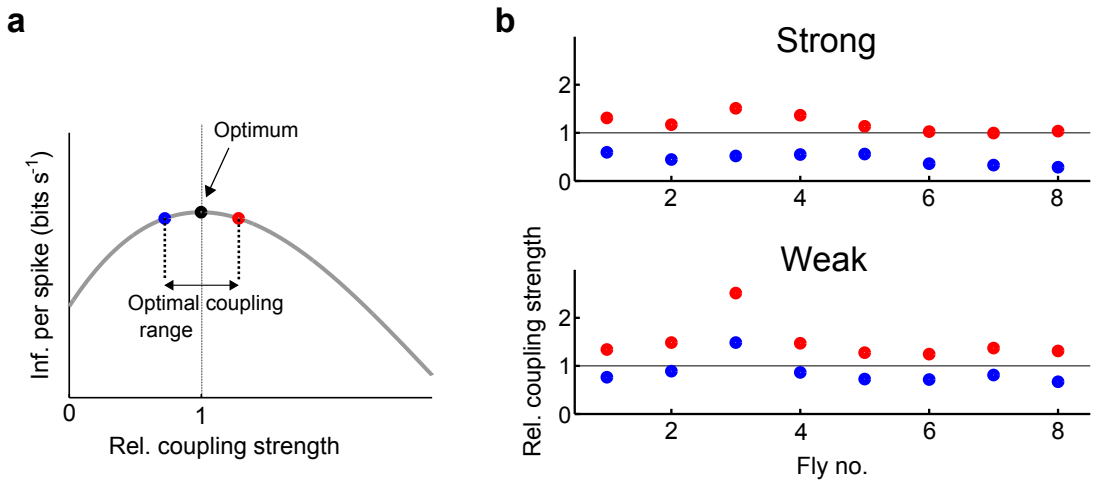

Supplementary Figure 6 (related to Figure 6)
Optimal Coupling Range for Single Flies.
(a) Fig. 6i depicts the information per spike as a function of the relative coupling strength. The resulting curves for strong and weak stimulation represent the average over eight flies. We found that the averaged information per spike curve is maximal for the measured coupling strengths. Here, we tested whether this finding also holds for each single fly instead of just the average. To this end, we fitted for each fly a third order polynomial to the information per spike curve. We then determined the relative coupling strengths left (blue) and right (red) to the optimum which are 1% worse than the maximal information per spike. The relative coupling strength is defined as the factor by which we varied the amplitude of the coupling filter (connecting H1 to Vi). Note that the *absolute* coupling strength differs for strong compared to weak stimulation, as the amplitude of the coupling filters decreases with increasing stimulation strength (see Fig. 4c-e).
(b) The blue and red points depict the coupling strengths left and right to the optimum. The y-axis depicts the factor by which the amplitude of the coupling filter was varied, i.e. 1 corresponds to the measured coupling strength. (Top) For strong stimulation, the measured coupling strength of all flies lies in the optimal coupling range (1% left and right to the optimum). (Bottom) For weak stimulation, all but one of the flies are in the optimal coupling range. Of note, fly 3 showed the weakest increase in the coupling filter amplitude, when reducing the stimulation strength from strong to weak. In average, during weak stimulation, the amplitude was enhanced by a factor of 1.42. In case of fly 3, the increase only amounted to 19%. Hence, this outlier demonstrates that the increase in the coupling gain is indeed required to make single spikes more informative during weak stimulation.

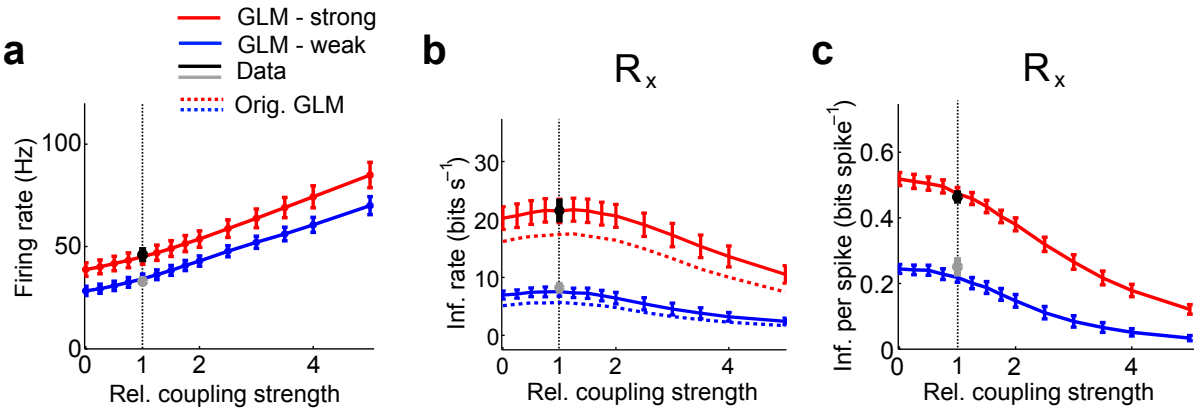

Supplementary Figure 7 (related to Figure 6)
Stimulus Representation by Vi for Uncorrelated Inputs from H1.
(a) Averaged mean firing rates of Vi in dependence of the coupling strength when uncorrelated rotation stimuli were presented to the left and right eye. To test whether the improved stimulus representation by Vi is due to the information about x-rotations provided by H1, we applied the same analysis as presented in Fig. 6 to the uncorrelated stimulus condition, where we presented two different (uncorrelated) random rotation stimuli on the left and right side of the stimulus device (see Methods, Random Rotation Stimulus), i.e. Vi and H1 receive uncorrelated stimulus input from their ipsilateral eye. Since the input provided by H1 is uncorrelated to Vi's activity, it is expected to impair Vi's stimulus processing. Error bars denote the S.E.M.
(b) Information of Vi about R_x during uncorrelated stimulation. Since increasing coupling strengths induce higher firing rates, Vi's information rate (measured in bits s^{-1}) is slightly increased for weak coupling strengths up to 1, an effect reminiscent of stochastic resonance [1]: H1's activity is uncorrelated to feed-forward inputs to Vi coming from the left eye. Since the coupling from H1 to Vi is purely excitatory, the uncorrelated input from H1 can be interpreted as a positive noise source lowering the spiking threshold in Vi. However, compared to Fig. 6d, the benefit of this effect is very weak. Moreover, for stronger couplings, the information rate is clearly deteriorated. These results demonstrate that the improved stimulus processing by Vi mainly relies on the finding that Vi and H1 are stimulus correlated due to their overlapping rotation tunings. The measured values are shown in black and gray. Error bars denote the S.E.M.
(c) Information per spike carried by Vi about R_x during uncorrelated stimulation. If H1 provides uncorrelated input to Vi, the information per spike is reduced with increasing coupling strength. Error bars denote the S.E.M.

B. Supplementary Results: Linear Two-Neuron Model

To gain a more intuitive understanding of the results presented in the main text, we analyzed a simplified, linear two-neuron model describing the interaction between Vi and H1 (see Fig. B.1a). The activity of neuron 1, modeling Vi, is proportional to the x-rotation velocity $R_x(t)$, intrinsic noise $\eta_1(t)$ and the lateral input from neuron 2 (H1). Assuming, for simplicity, that the coupling between both neurons is linear, the activity of neuron 1 can be expressed as

$$r_1(t) = R_x(t) + \eta_1(t) + c\, r_2(t), \tag{1}$$

where the parameter c determines the strength of the coupling between neuron 1 and neuron 2. The preferred rotation axis of H1 (neuron 2) is a linear combination of the x- and z-axis (see Supplementary Fig. 1c). In the following the coordinates with respect to the x- and z-axis are denoted by a and b, with $a^2 + b^2 = 1$. The larger a, the stronger neuron 1 and neuron 2 are correlated with respect to x-rotations. With $\eta_2(t)$ describing the noise in neuron 2, the activity of neuron 2 is given by

$$r_2(t) = (aR_x(t) + bR_z(t))\,\sqrt{g} + \eta_2(t). \tag{2}$$

To account for differences in the signal powers of both neurons, we introduced the parameter $g = Sig_2/Sig_1$, where Sig_i is the signal power in the activity of neuron i. Without coupling (i.e. $c = 0$), $Sig_1 = \langle R_x(t)^2 \rangle$, where the angular brackets denote averaging over time. In the following, we will drop the parameter t for notational convenience. Combining Equations 1 and 2 yields

$$r_1 = \underbrace{R_x(1 + c\,a\sqrt{g})}_{signal} + \underbrace{\eta_1 + c(b\sqrt{g}R_z + \eta_2)}_{noise}. \tag{3}$$

The first term in Equation 3 captures the encoded signal, while the second term describes noise potentially impairing the stimulus representation. The noise term comprises the noise present in both neurons and information about z-rotations. Increasing the coupling (i.e. the parameter c) strengthens the power of the encoded signal R_x by the factor $c\,a\sqrt{g}$. However, larger values of c simultaneously enhance the noise term, which might deteriorate the encoding of R_x and shift the stimulus tuning of neuron 1 due to the increased contribution of R_z.

Fig. B.1b shows the information carried by the response of neuron 1, r_1, which was calculated according Equation 3. To quantify the information, we reconstructed the stimulus from the activity of neuron 1 using linear decoding (as we did for Fig. 6). The noise terms were modeled by Gaussian white-noise. For strong and weak stimulation, the variances of η_1 and η_2 as well as of the variances of the signals, Sig_1 and Sig_2, were set to the values experimentally measured for Vi and H1. The parameters a and b equal the coordinates of H1's preferred rotation axis with respect to R_x and R_z (see Supplementary Fig. 1c). For both stimulus conditions, the information about R_x carried by r_1 shows a similar dependence on the coupling strength as found for the spike trains

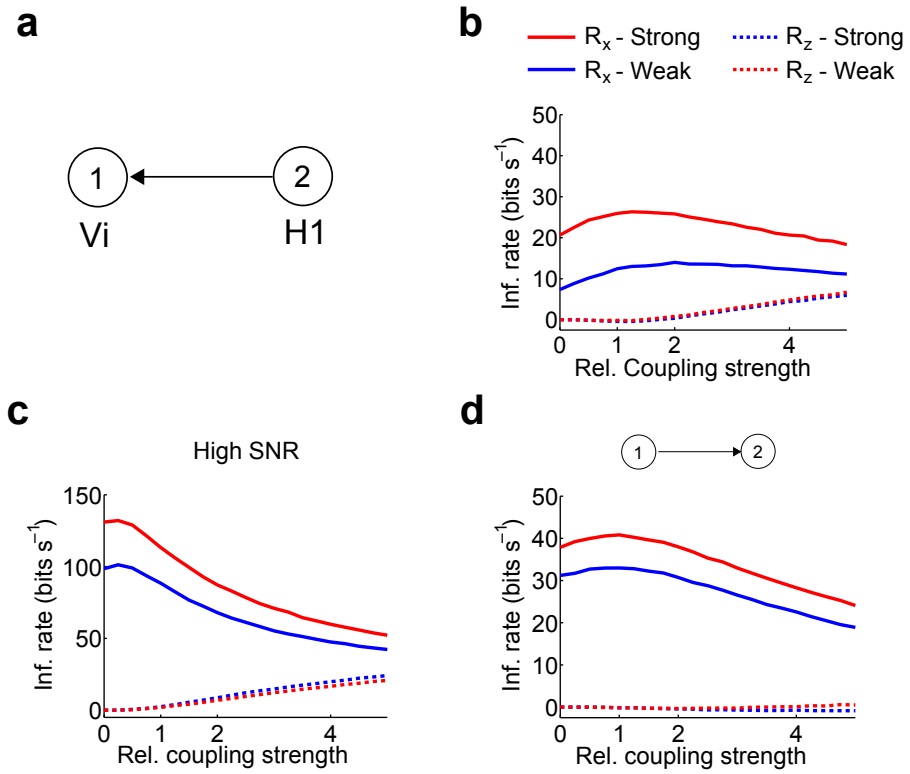

Figure B.1. Linear Two-Neuron Model. **(a)** In the linear model, neuron 1's activity is proportional to the x-rotation velocity, R_x, while neuron 2's activity is proportional to a weighted sum of R_x and R_z. **(b)** The linear model reproduces the dependence of the information rate of neuron 1 on the coupling strength as found for the spike trains simulated by the GLMs (see Fig. 6d,f. The values of the signal and noise variances of neuron 1 and 2 were set to the values experimentally measured for Vi and H1. **(c)** At high SNR, neuron 1 benefits less from a coupling. Moreover, the optimal coupling strength is reached for smaller values. Compared to the values in **(a)**, the SNR was increased by a factor of 5. **(d)** Information carried by neuron 2 about rotations around its preferred rotation axis. For the signal and noise variances the same values were used as in **(a)**.

generated by the GLMs (see Fig. 6d). The information about R_z is shown by the dotted lines. As shown for the spike trains predicted by the GLM, for weak coupling strengths ($c < 1.5$), neuron 1 contains no information about R_z (compare Fig. 6f). Hence, this simple linear model captures one major finding: For weak couplings, inputs from neuron 2 (H1) to neuron 1 (Vi) do not affect the shape of neuron 1's original stimulus tuning. Hence, this phenomenon is not due to a nonlinearity in the GLM, but seems to be a consequence of summing signals under noise. For weak couplings, neuron 1 contains no information about z-rotations, since R_z is simply masked by the noise terms η_1 and $c\,\eta_2$. However, if the coupling is too strong, R_z becomes more and more pronounced in the signal. Fig. B.1c shows the information carried by r_1 at high SNR. In this case, the optimal coupling strength is reached for smaller values and neuron 1 benefits less from inputs from neuron 2. Fig. B.1d shows the information carried by neuron 2 about its preferred rotation axis in dependence of increasingly strong inputs provided by neuron

1. Since neuron 2 (H1) has a significantly larger SNR under both stimulus conditions (see Fig. 2e), it benefits much less from inputs by neuron 1 than vice versa (compare Fig. 7).

Comparison of Fig. B.1b and B.1c suggests that the difference in the SNRs of neurons 1 and 2 determines to what degree one neuron can benefit from the second one. How does the optimal coupling strength from neuron 2 to 1 depend on the SNRs of both neurons? To address this question, we calculated how the coupling influences the SNR of neuron 1, which is closely related to the information encoded in the neuron's activity [2]. The SNR of neuron 1 as a function of the coupling strength c can be expressed as

$$SNR_1(c) = \frac{\langle R_x^2\rangle(1+ac\sqrt{g})^2}{\langle \eta_1^2\rangle + c^2b^2g\langle R_z^2\rangle + c^2\langle \eta_2^2\rangle}, \tag{4}$$

where we made use of the independence of the signals R_x and R_z. To find the coupling strength c which maximizes $SNR_1(c)$, we set the derivative of $SNR_1(c)$ with respect to c to zero and solved for c. The coupling strength c_{max}, which maximizes $SNR_1(c)$ is given by

$$c_{max} = \frac{a\sqrt{g}\langle \eta_1^2\rangle}{b^2g\langle R_z^2\rangle + \langle \eta_2^2\rangle}. \tag{5}$$

For simplicity, we assume that $\langle \eta_1^2\rangle = \langle \eta_2^2\rangle$, which is indeed the case for Vi and H1. (The differences in the SNRs of Vi and H1 are determined by differences in the signal and not the noise power). Further calculations then yield the following expression for c_{max},

$$c_{max} = \frac{a}{\sqrt{SNR_1(0)}\ \left(\sqrt{SNR_2}\ (1-a^2)+1\right)}, \tag{6}$$

where $SNR_1(0)$ describes the SNR of neuron 1 without coupling, i.e. $c = 0$. The SNR of neuron 2 is referred to as SNR_2. Equation 6 states that with increasing values of the SNRs of both neurons, the optimal coupling strength decreases. This effect is in compliance with the finding that, for weak stimulation, the gain of the coupling filter from H1 to Vi is increased compared to strong stimulation (see Fig. 4c-e).

Next, we addressed the question under which condition neuron 1 maximally benefits from neuron 2. To this end, we considered the percentage by which $SNR_1(c_{max})$ is increased compared to $SNR_1(0)$. First, $SNR_1(c_{max})$ can be expressed as

$$SNR_1(c_{max}) = \frac{b^2g\langle R_x^2\rangle\langle R_z^2\rangle + \langle R_x^2\rangle\left(a^2g\langle \eta_1^2\rangle + \langle \eta_2^2\rangle\right)}{b^2g\langle \eta_1^2\rangle\langle R_z^2\rangle + \langle \eta_1^2\rangle\langle \eta_2^2\rangle}. \tag{7}$$

The percentage by which SNR_1 is increased through an optimal coupling can then be written as

$$\Delta_{max}SNR_1(c_{max}) = \frac{SNR_1(c_{max}) - SNR_1(0)}{SNR_1(0)} = \frac{a^2g\langle \eta_1^2\rangle}{b^2g\langle R_z^2\rangle + \langle \eta_2^2\rangle} \tag{8}$$

Further calculation finally yields,

$$\Delta_{max}SNR_1(c_{max}) = \frac{a^2SNR_1(0)^{-1}}{(1-a^2) + {SNR_2}^{-1}}. \tag{9}$$

Hence, the smaller the SNR of neuron 1 compared to the SNR of neuron 2, the more neuron 1 will benefit from neuron 2. In contrast, if the SNR of neuron 2 is significantly larger than $SNR_1(0)$, neuron 2 will not profit from an interaction with neuron 1 as observed, when coupling Vi to H1 in the GLM (see Fig. 7).

In the end, we have to emphasize that there are still issues to be solved before we can directly relate the calculation done for the linear two-neuron model to the GLM of Vi and H1. First, the linear model works with continuous signals, while all analysis for the GLM is based on spike trains. Accordingly, here we optimized the SNR, while in case of the GLM the information per spike was found to be maximal. Second, the linear model does not account for nonlinearities present in the GLM as the spiking nonlinearity or the purely excitatory connection from H1 to Vi acting as a half-wave rectifier. Finally, there is no direct relation between the SNR of a neuron in the linear model and the SNR of a GLM, since in the GLM the same SNR can be obtained by a large variety of different parameter combinations. Nevertheless, the linear model allows for a more general understanding of how Vi and H1 should be coupled, and will probably be the starting point for any more thorough analysis.

[1] K. Wiesenfeld and F. Moss. Stochastic resonance and the benefits of noise: from ice ages to crayfish and squids. *Nature*, 373(6509):33–36, 1995.

[2] A. Borst and F. E. Theunissen. Information theory and neural coding. *Nat Neurosci*, 2(11):947–957, 1999.